Site occupancy and near-infrared luminescence in $Ca_3Ga_2Ge_3O_{12}$: Cr^{3+} persistent phosphor

Huihong Lin, Gongxun Bai, Ting Yu, Ming-Kiu Tsang, Qinyuan Zhang, Jianhua Hao**

Dr. H.H. Lin, Dr. G.X. Bai, M.-K. Tsang, Prof. J.H. Hao*

Department of Applied Physics

The Hong Kong Polytechnic University

Hong Kong, China

E-mail: jh.hao@polyu.edu.hk

Dr. H.H. Lin, T. Yu, Prof. Q.Y. Zhang*

State Key Laboratory of Luminescence Materials and Devices

Institute of Optical Communication Materials

South China University of Technology

Guangzhou 510641, China

E-mail: qyzhang@ scut.edu.cn

Dr. G.X. Bai, M.-K. Tsang, Prof. J.H. Hao*

The Hong Kong Polytechnic University Shenzhen Research Institute

Shenzhen 518057, P. R. China

Keywords: near-infrared luminescence, site occupancy, persistent, energy transfer

Abstract: The near-infrared (NIR) luminescence properties of Cr^{3+} activated $Ca_3Ga_2Ge_3O_{12}$ (CGGG) have been studied under ultraviolet and visible light excitation. Three types of Cr^{3+} centers associated with $^4T_2$-$^4A_2$ transition resulting in the emissions located at 650-1100 nm are identified in all Cr^{3+}-doped samples. Thanks to the occupancy of three non-equivalent sites in CGGG, we observed NIR luminescence peaking at about 749, 803, and 907, respectively. The influence of crystal field on site occupancy is studied, the relation between site occupancy and the NIR luminescence is addressed, energy transfer process among Cr^{3+} sites and the decay behaviors for Cr^{3+} in different sites are evaluated. It is found that a superior NIR/persistent luminescence comes from the traps that Cr^{3+} enters Ga^{3+} site. The results are of benefit to investigate Cr^{3+} activated persistent phosphors.

1. Introduction

Chromium exists as Cr^{3+}, Cr^{4+}, and Cr^{6+} in compounds, and is mostly dominant by +3 oxidation states because of the most stable outer electronic configuration of Cr^{3+} [Ar]$3d^3$. On the basis of electronic structure, the unfilled $3d^3$ electronic shell of the Cr^{3+} ion splits into a number of low-lying energy levels, among which photon transitions can arise generating luminescent emission. Therefore, Cr^{3+} is extensively utilized as active ions and sensitizers in numerous materials for solid state lasers and optoelectronic devices.[1,2]

Persistent luminescent materials can store excitation energy in a trap(s) and then an activator can release it by luminescence through thermal or mechanical stimulation for a while which is much longer than the lifetime of the luminescent state.[3] In particular, near-infrared (NIR) luminescence in the region between 800 nm and 2500 nm has many technological applications, such as optical telecommunications, photon management for solar energy, and biomedical imaging.[4] In recent years, much attention has been focused on NIR long-lasting persistent luminescent phosphors as optical probes in biomedical imaging applications.[5] For these applications, it is essential to employ a appropriate emitter capable of generating NIR

photon and an suitable host capable of creating traps of suitable depth and promoting persistent luminescence.

To obtain efficient NIR emission, trivalent chromium (Cr^{3+}) is preferentially chosen as a favorable luminescent centre in solids, because it exhibits narrow-band emissions (usually near 700 nm) due to the spin forbidden ^2E---$^4A_2$ transition, or a tunable broadband emission (650-1600 nm) originating from the spin-allowed $^4T_2$---$^4A_2$ transition, which strongly depends on the crystal-field environment of the host lattices. Recently, numerous studies have been reported about the NIR luminescence of Cr^{3+} in various materials, such as $Zn_3Ga_2Ge_2O_{10}:Cr^{3+}$, $Zn(Ga_{1-x}Al_x)_2O_4:Cr^{3+},Bi^{3+}$, $ZnGa_2O_4:Cr^{3+}$, $La_3Ga_5GeO_{14}:Cr^{3+}$, $LiGa_5O_8:Cr^{3+}$, etc.[6-10]

The selection of $Ca_3Ga_2Ge_3O_{12}$(i.e., $Ca_3Ga_2(GeO_4)_3$,CGGG) as a host for dopants is based on the easy incorporation of transition metal ions such as Cr^{3+} into the host through substitution at the Ga^{3+} site. This garnet host crystallizes in the space group *Ia*-3*d* (*Z* = 2) with Ca^{2+} ions situated at D_2 sites and Ga^{3+} at C_{3i} sites. Most of the previous studies utilizing this host lattice have been performed using Nd^{3+} as the dopant ion.[11-15] The substitution of the trivalent ion at the Ca site results in six non-equivalent Nd^{3+} sites in the disordered crystal.[11] In spite of this complication, the Nd^{3+}-doped crystal has been employed as an optical pressure sensor.[12] Infrared to visible upconversion has also been observed in $Ca_3Ga_2Ge_3O_{12}:Nd^{3+}$.[14] Upconversion was also observed in the Cr, Yb, Tm tri-doped phosphor, together with Cr^{3+} persistent luminescence.[16] Xia et al. found that the persistent luminescence decay time of $Ca_3Ga_2Ge_3O_{12}:Cr^{3+}$ could be extended by co-doping with Bi^{3+}.[17] Recently, we found that CGGG:Cr^{3+},Nd^{3+} presents more excellent NIR long-lasting persistent performance than Cr^{3+} singly doped CGGG through producing the deeper traps to store more.[18] It is known for the excellent NIR long-lasting persistent materials, the afterglow mechanism that is a crucial issue, involved the trapping and de-trapping process, should be well understood. In general, the involved traps derive from some lattice defects, *i.e.* intrinsic defects, intentionally introduced defects or both.[19,20] On the other hand, for persistent materials, near-infrared luminescent

properties at different lattice sites are of great importance for most selective applications, because they are tunable theoretically. Here, Cr^{3+}-doped CGGG is a typical example, at least three types of Cr^{3+} centers located at 650-1100 nm, which could provide an opportunity on deep investigation. Therefore, the site occupancy and the persistent luminescence of Cr^{3+} at different sites in CGGG will be addressed in this work.

2. Results and Discussion

2.1. The site occupancy luminescence of Cr^{3+} in $Ca_3Ga_2Ge_3O_{12}$

The emission spectra of a series phosphors $Ca_3Ga_{2-x}Cr_xGe_3O_{12}$ (x = 0.005, 0.01, 0.03, 0.05, 0.07, 0.10) were measured. As an example, we first present the NIR emission spectra of $Ca_3Ga_{2-x}Cr_xGe_3O_{12}$ for x = 0.01, 0.05, 0.10 under 267 nm excitation (host-related absorption band) at room-temperature (RT), respectively, shown in Figure1.

The electron configuration for Cr^{3+} is $1s^22s^22p^63s^23p^63d^3$, thus the Cr^{3+} ion is a d^3 transition metal ion. The optical properties of Cr^{3+} ion in crystals are analyzed using by the so-called Tanabe-Sugano diagrams as the standard reference data. In general, when Cr^{3+} lies in stronger crystal field site, the energy $^2E<{}^4T_2$, fluorescence spectra show obvious sharp lines; on the contrary, when it is in weaker crystal field site, the energy $^2E>{}^4T_2$, only $^4T_2$ broadband emission spectra can be observed.

From Figure 1(a), one can see an ultra-broadband NIR (670-1100 nm) emission spectrum composed of three peaks. The change in relative intensities of these three features with Cr^{3+} concentration shows that there are at least three different Cr^{3+} centers in the crystal. The spectrum can be fitted well with a sum of three Gaussian profiles, marked as I (~ 749 nm), II (~ 803 nm) and III (~ 907 nm), respectively. It indicates that three types of Cr^{3+} centers attributed to $^4T_2$-$^4A_2$ transition occur, labeled as Cr(1), Cr(2), and Cr(3), also shown in Figure 1. The 453-nm excited RT spectrum of $Ca_3Ga_{1.94}Cr_{0.06}Ge_3O_{12}$ in the region from 600-850 nm has previously been reported by Liu et al.[17] Two broad bands were observed in this spectral

region by these authors, in agreement with the present study, but we prefer the assignment of the luminescent state for this broadband emission as $^4T_2$ rather than ^2E. In the CGGG crystal structure, each cation of Ca^{2+}, Ga^{3+}, and Ge^{4+} occupies one kind of crystallographic sites. Though Cr^{3+} substitutes Ga^{3+} site are expected to occur in the samples of $Ca_3Ga_{2-x}Cr_xGe_3O_{12}$ according to the formula of the compounds, however, at least three Cr^{3+} emission peaks are found in all Cr^{3+}-doped samples, suggesting that Cr^{3+} occupied three non-equivalent sites in CGGG, Ca^{2+}, Ga^{3+}, and Ge^{4+} sites or others.

Figure 1 (b) illustrates the NIR emission spectra of the samples $Ca_3Ga_{1.99}Cr_{0.01}Ge_3O_{12}$ under 267, 460, 640 nm excitation at RT, respectively. It can be found that there appear similar spectroscopic properties with those in Figure 1(a). Under the excitation at different wavelengths, three types of Cr^{3+} centers [e.g. Cr(1), Cr(2), and Cr(3)] in all spectra occur. The relative intensities of three Cr^{3+} sites have a corresponding change under 267, 460, 640 nm excitation, respectively (not shown here). Obviously, under the same doping concentration, it is in favor of longer wavelength [Cr(3)] emission upon 267 nm excitation. It reveals that energy transfer from the host to Cr(3) is more efficient. At the same time, we notice that the ratio of relative intensities $I_{Cr(3)/Cr(1)-Cr(2)}$ also increases when increasing Cr^{3+} doping concentration under the excitation at 267 nm, which indicates that the higher the doping concentration, the stronger Cr(3) emission intensities. These phenomena fully shows the relative low energy Cr site is related to the host and the doping Cr concentration, which will discuss in the following section in detail.

It is worth noting that only broadband emission spectra can be observed in all Cr^{3+}-doped samples at RT. So, we can confirm that Cr^{3+} ions occupy the site with relatively weaker crystal field in CGGG. As above mentioned, in the structure of CGGG, as shown in Figure 1(c), the configurations of Ca^{2+}, Ga^{3+}, and Ge^{4+} are dodecahedral, octahedral, and tetrahedral respectively. The order of the crystal field strength is tetrahedral > octahedral > dodecahedral. On the basis of the mean peak energy of the $^4A_2$ --- $^4T_2$ transition, we could obtain the value

of the local crystal-field parameter D_q and the Racah parameter B. It was calculated the value of D_q/B for Cr^{3+} in the CGGG host is 2.40, which is consistent with the result reported by Chen. At the same time, it is suggested that Cr^{3+} is at intermediate field sites. Therefore, Cr^{3+} maybe prefer to occupy Ca^{2+}, Ga^{3+} in CGGG host. When Cr^{3+} ions substitute Ca^{2+} dodecahedral c-lattice ions, the compensation of the excess charge of the Cr^{3+} ions can be performed by Ga^{3+} ions substituting Ge^{4+} tetrahedral d-lattice ions. Thus, the disorder is introduced into the host lattice due to the possibility of formation of different types of Cr^{3+} (Ca^{2+})-Ga^{3+} (Ge^{4+}) associations. Therefore, different Cr^{3+} centers occur, as shown in Figure 1, Cr(1), Cr(2), and Cr(3), respectively.

The NIR emission spectra of the samples $Ca_3Ga_{1.99}Cr_{0.01}Ge_3O_{12}$ under 467 nm excitation at 10 K, 100 K, and 300 K are displayed in Figure 2 (a). At 10 K, several narrow emission bands (assigned to the Cr^{3+} ^2E – $^4A_2$ transition) are superimposed on broad emission band. Between 100 K and 10 K, the high energy part of the emission spectrum becomes structured, with peaks at 702.8, 723 and 742 nm. This structure is associated with the ^2E --- $^4A_2$ transition, with the zero phonon line (at 14228 cm^{-1}) corresponding to the first feature and the other bands to members of the vibrational progression in the Cr-O stretch mode of 353 cm^{-1}. There was not major change in the relative intensities of the broad bands on cooling. This indicates (i) in this case the highest energy emission is not associated with the $^2T_1$ --- $^4A_2$ transition, as assigned in $MgGa_2O_4$ – Ga_2O_3 doped with Cr^{3+} ions;[21] and (ii) the efficiency of energy transfer between the Cr^{3+} sites is weak. With the increase of the temperature, sharp emission peaks gradually disappear, and no sharp emission peaks occur at 300 K. Similarly, three types of Cr^{3+} centers [e.g. Cr(1), Cr(2), and Cr(3)] appear all different temperature spectra.

Figure 2 (b) shows variable temperature emission spectra of $Ca_3Ga_{1.99}Cr_{0.01}Ge_3O_{12}$ under the excitation at 269 nm. Generally, luminescent material may occur thermal quenching by many reasons, but play a key role in two ways as follows. First, the lattice vibration becomes

intensify with the temperature increases, so that the luminous center of the lattice relaxation enhance, non-radiation transition probability increases with reducing the luminous efficiency, which is commonly referred to "temperature characteristics"; Secondly, the light emitting center of the state or the surrounding micro-environment makes some essential changes to reduce the luminous efficiency, which commonly referred to "thermal stability." In Figure 2(b), we can find that the Cr emission intensities increase with the increase of temperature from 10K to 300 K, including three Cr sites. This maybe gives us a note that some traps or defects are involved in this elevated temperature process. It was reported that Cr^{3+} activated $Ca_3Ga_2Ge_3O_{12}$ (CGGG) has long lasting persistent luminescence, [16] which is consistent with our results.

The excitation spectra of the sample $Ca_3Ga_{1.99}Cr_{0.01}Ge_3O_{12}$ under 749, 803, and 907 nm emissions at RT are shown in Figure 3. They show similar spectral profile except for the difference in relative intensity, suggesting that similar crystal field environment of three types of Cr^{3+} centers or energy transfer between two occurring. From the results of EPR and the decay lifetime, as shown in the follow, we consider that the reason behind the observation is the energy transfer from Cr(1) to Cr(2) or from Cr(2) to Cr(3). Here, we could speculate that Cr(1) is associated with Cr^{3+} entering onto Ga^{3+} site, while Cr(2)/ Cr(3) are associated with Cr^{3+} (Ca^{2+})-Ga^{3+}(Ge^{4+}) associations, which belong to defect sites. Four broad bands peaked at about 247, 310, 460, 640 occur in excitation spectra, labeled as A, B, C, and D, respectively. Because of the limit of measurement instrument, the test of excitation spectra only begin at 250 nm, the band A (~ 247 nm) can not be displayed in Figure 3. But we can estimate the location is at about 247 nm based on the inset of Figure 3 (a), which is ascribed to the absorption of the CGGG host. The bands B, C, and D are attributed to the $^4A_2$---$^4T_1$(^4P), $^4A_2$---$^4T_1$(^4F), and $^4A_2$---$^4T_2$(^4F) transitions of Cr^{3+}, respectively. The inset of Figure 3 (b) shows the diffuse reflection spectrum of $Ca_3Ga_{1.99}Cr_{0.01}Ge_3O_{12}$, all the observed absorption peaks agree well with the electronic transitions of Cr^{3+} ion.

Cr^{3+} ion has electronic spin S = 3/2 and nuclear spin I = 3/2 or 0, depending on the isotopes. In $3d^3$ electronic configuration, a total spin S = 3/2 is resulted from the outer three electrons occupying the d-orbitals. So, these three electrons are responsible for the signals in the EPR spectrum.[22] Here, it is worth noting that when there is an external magnetic field, the degenerate doublets split further. By applying an external magnetic field, a transition with $\Delta m_s = \pm 1$ may be observed in the EPR spectra. The number of signals depends upon the magnitude of the zero field splitting for a given photon energy. The EPR spectra of the samples $Ca_3Ga_{2-x}Cr_xGe_3O_{12}$ (x = 0, 0.01, 0.05, 0.10) measured at 100 K display in Figure 4. The obvious signal at g = 3.93 can be assigned to the isolated Cr^{3+} ions in strong ligand field sites. The signal at g = 2.04 which is attributed to exchange coupled Cr^{3+}-Cr^{3+} ion pairs in weak ligand field sites, is very weak in Cr^{3+} doped samples. From the Figure 4, it can be observed that the chromium ions are in 3+ oxidation state.

To identify the substitution site location of the Cr^{3+} ion in the CGGG crystal, we considered the following several points. Firstly, The approximate ionic radii of Ca^{2+}, Ga^{3+}, and Ge^{4+} cations in CGGG are as follows: Ca on dodecahedral site (CN = 8, r = 1.12 Å); Ga on octahedral site (CN = 6, r = 0.62 Å); Ge on tetrahedral site (CN = 4, r = 0.53 Å). The ionic radius of the Cr^{3+} ion is 0.62 Å for a coordination number of 6, then, it is reasonable to assume that the doped transition metal Cr^{3+} ion easily prefer to occupy Ga^{3+} the octahedral site of Ga^{3+} in the CGGG host because of their similar ionic radii. Secondly, it is inevitable that a bit Cr^{3+} ion enters larger Ca^{2+} sites, which is a non-equivalent substitution. To balance the excess charge of the Cr^{3+} ions, Ga^{3+} ions substituting Ge^{4+} tetrahedral d-lattice ions will be promoted. Thus, disorder might be introduced into the host lattice due to the possibility of forming different types of Cr^{3+} (Ca^{2+})-Ga^{3+} (Ge^{4+}) associations. Therefore, it can be concluded that two sets of magnetically in equivalent resonance lines for the Cr^{3+} ion. Fortunately, our measurements on CGGG:Cr^{3+} samples show two set of resonance lines, as shown in Figure 4. Then, it is reasonable to assume that the strong signal observed at g = 3.93

is ascribed to Cr^{3+} in Ga^{3+} sites, while the sharp signal observed at g = 2.04 is ascribed to Cr^{3+} in $Cr^{3+}(Ca^{2+})$-$Ga^{3+}(Ge^{4+})$ sites, which should yield identical EPR spectra due to the crystal symmetry.

2.2. NIR persistent luminescence of Cr^{3+} in $Ca_3Ga_2Ge_3O_{12}$

Figure 5 (a) shows the three-dimensional TL spectra of the samples $Ca_3Ga_{2-x}Cr_xGe_3O_{12}$ (x = 0.01, 0.05, 0.10 from top to bottom) after 254 nm excitation for 5 min. Because of the limitation of the equipment, the test of emission wavelength only ends at 800 nm, not all the Cr^{3+} emissions, including Cr(1), Cr(2), and Cr(3), can be displayed in Figure 5(a). Here, we can estimate persistent luminescence in Figure 5 (a) comes from Cr(I) site (~750 nm). With the increase of Cr^{3+} concentration, from top to bottom, it can be found that the intensity of LLP become weaker and weaker. Hence, the optimum concentration for Cr(I) site LLP is x = 0.01. And, the image in top right corner of every graph is from the background. Figure 5 (b) shows the LLP decays of Cr: CGGG phosphors doped with various Cr^{3+} contents monitored at 750 nm emission after 254 nm light illumination for 5 min. The results presented temporal dependence of the LLP intensity, and the recording time lasted for 7000 s. The LLP intensity decreases quickly in 3500 s and then decays very slowly. When the content of Cr^{3+} increases, the decay rate of LLP becomes faster because of concentration quenching. As revealed in Figure 5 (c), the TL curves of Cr:CGGG consists of three broad bands with maxima at about 75, 200 and 320 °C, which correspond to the shallow and deep traps, respectively. As an example, the Gauss fit peaks of the sample $Ca_3Ga_{1.99}Cr_{0.01}Ge_3O_{12}$ shows the inset of Figure 5 (c), marked as I (~ 88 °C), II (~182 °C), III (~241°C), and IV (~317°C), corresponding to the shallow and deep traps, respectively. The thermal activation energy E of trapped carriers, which corresponds to the trap depth, can be estimated by Hoogenstraaten method. According to the fomula, $E = 2kT_m^2/\omega$, the values of E are 0.70 eV (peak I), 0.81 eV (peak II), 1.38 eV

(peak III) and 1.45 eV (peak IV) are obtained. [23] These results are consistent with the reported.[16, 17]

2.3. The decay curves for Cr^{3+} in different sites

Figure 6 shows the decay curves of $Ca_3Ga_{1.99}Cr_{0.01}Ge_3O_{12}$ upon 470 nm excitation with different emission wavelength of Cr^{3+} sites at RT. It can be observed that the decay time decreases with the red-shift of emission wavelength. The value of Cr(1), Cr(2) and Cr(3) lifetime is 144, 122 and 93 μs, respectively. As mentioned above, energy transfer between Cr sites occurs. So, we consider that the decay time of Cr(1) is the shortest, while Cr(3) is the longest. But actually just the opposite. We can analyze from the following issue. Low energy sites Cr(2) and Cr(3) are related with $Cr^{3+}(Ca^{2+})$-$Ga^{3+}(Ge^{4+})$ associations, which easily produce a lot of defects. Energy transferring and defects quenching are two competing processes. Here, it is clear that defects quenching dominates the process.

Figure 7(a, b) displays the decay curves of $Ca_3Ga_{1.99}Cr_{0.01}Ge_3O_{12}$ upon 467 nm excitation with emission wavelengths at 765 nm [Cr(1)] and 920 nm [Cr(3)] in the temperature range of 10-300 K. It can obviously observed that the decay rate of these two sites is different. The curves demonstrate that Cr^{3+} ions in Cr(3) sites are with a rather high decay rate. See (a), with the increase of temperature, the lifetime of Cr(1) site becomes shorter and shorter, especially above 100 K. While the lifetime of Cr(3) site basically does not change with temperature, keep constant. These curves can be well fitted by a bi-exponential equation (1),

$$I_t = I_0 + A_1 \exp(-t/\ _1) + A_2 \exp(-t/\ _2), \quad (1)$$

where I is the luminescence intensity, A_1 and A_2 are constants, t is the time, and T_1 and T_2 are the decay times for the bi-exponential components, respectively. Furthermore, the lifetime of the nonexponential decay curve is determined by the expression $_{ave} = \frac{A_1\ _1^2 + A_2\ _2^2}{A_1\ _1 + A_2\ _2}$. As examples, the T_{ave} values of these inset four curves are calculated from the fitted curves with

288 and 151 μs (a), 109.5 and 109.7μs (b), respectively. It is found that the decay lifetime of highest energy site Cr(1) is the longest whatever at RT or 10 K, which seem to indicate energy transfer from high energy sites to low that is not efficient. Otherwise, with the increase of temperature, the lifetime of three Cr^{3+} sites increases at a different degree. This phenomenon is different from general routine.

Based on the above results, we proposed the schematic electronic energy levels of Cr^{3+} ions together with traps/defects in the CGGG host depicted in Figure 8. According to the above discussion, Cr(1) is attributed to Cr^{3+} in Ga^{3+} sites, producing a broad band peaked at 749 nm, which dominates the NIR emission intensities. Cr(2)/Cr(3) are attributed to Cr^{3+} in $Cr^{3+}(Ca^{2+})$-$Ga^{3+}(Ge^{4+})$ sites, producing at least two broad bands peaked at about 803 and 907 nm. With the excitation at 267 nm (HA), energy transfer from the host to Cr(1), Cr(2) and Cr(3) is all efficient, which it can be observed three Cr sites emissions, as shown in Figure 1. When excitation at 460/640 nm [$^4A_2$---$^4T_1(^4F)$ and $^4A_2$---$^4T_2(^4F)$ transitions of Cr^{3+}], three Cr sites emissions also can be observed, but Cr(2)/Cr(3) emissions obviously become weak relative to Cr(1). We consider that the results of competition on energy transferring among Cr sites and defects/traps quenching. As an example, the optimal doping concentration of Cr(1) is about $x = 0.01$, while the optimal doping concentration of Cr(3) is much larger than 0.01. It is observed that higher doping concentration, stronger defects emission in our doping concentration range. In general, defects luminescence and quenching are one pairs competition, which affect with the host, impurity doping concentration, the temperature, etc. In short, according to the energy level of Figure 8, we can draw the following points. Cr^{3+} activated CGGG phosphors are good NIR persistent luminescence materials. Cr(1) site (~749 nm) is produced by Cr^{3+} replace Ga^{3+}, such substitution match the lattice better, then it does not have a lot of defects. While, Cr(2) (~803 nm) and Cr(3) (~907 nm) sites is produced by $Cr^{3+}(Ca^{2+})$-$Ga^{3+}(Ge^{4+})$ associations, which will generate many defects. Therefore the NIR persistent luminescence of Cr(2) and Cr(3) sites certainly is a better character. Due to the

restrictions the experimental apparatus, we cannot examine the three-dimensional thermo-luminescence spectra of Cr(2) and Cr(3) sites. But our experimental results show that the defects/traps play a more important role on NIR luminescence.

2.4. Cathode-ray Luminescence (CL)

To confirm whether the multi-sites luminescence of Cr^{3+} in CGGG at high energy excitation, we measure the emission spectrum of the sample $Ca_3Ga_{1.99}Cr_{0.01}Ge_3O_{12}$ under cathode-ray excitation, as shown in Figure 9. It can be observed a obvious Cr^{3+} emission band, which can be fitted well with a sum of two Gaussian profiles, marked as ~ 732 nm [Cr(1)] and ~ 774 nm [Cr(2)], because of the limitation of the equipment. The inset shows the photo of $Ca_3Ga_{1.99}Cr_{0.01}Ge_3O_{12}$ under cathode-ray excitation with 5 KV power, in which bright red light can be seen by the naked eyes.

3. Conclusions

Ultra-broadband NIR persistence emission (~670-1100 nm) composed of three peaks centered at 749, 803, and 907 nm can be achieved in $Ca_3Ga_2Ge_3O_{12}$ (CGGG):Cr^{3+}. The Cr(1) is attributed to Cr^{3+} in Ga^{3+} sites with a broad band peaked at 749 nm, which dominates the NIR emission intensities. The Cr(2)/Cr(3) are attributed to Cr^{3+} in $Cr^{3+}(Ca^{2+})$-$Ga^{3+}(Ge^{4+})$ sites with at least two broad bands peaked at about 803 and 907 nm. The decay curves of different sites indicate that two competing processes, namely energy transfer and defects quenching are involved. We can tune NIR persistent luminescence by the methods of changing doping concentration and excitation wavelength. Cr^{3+} activated CGGG phosphors are attractive NIR persistent luminescence materials. Bright red emission can be obtained under cathode-ray excitation.

4. Experimental Section

Instrumentation: A Philips PW1830 X-ray powder diffractometer (XRD) with a Cu Ka (A = 1.54056Å) radiation at 40 kV and 40 mA was used to indentify phases identification of the obtained product. The XRD patterns of all samples $Ca_3Ga_{2-x}Cr_xGe_3O_{12}$($x$ = 0, 0.005, 0.01, 0.03, 0.05, 0.07, 0.10) are in good agreement with the CGGG standard card (JCPDS 11-0023).[18] This suggests that the substitution of Ga^{3+} by Cr^{3+} does not significantly influence the crystal structure. Steady-state photoluminescence (PL) spectra were recorded on an Edinburgh FLS920 spectrofluorimeter where an continuous wave 450 W xenon lamp was used as the excitation source, and the infrared emission was detected by a liquid-nitrogen cooled R5509-72 NIR PMT. Besides, temporal fluorescence spectra, such as decay curves and time-resolved emission spectra were additionally recorded on the FLS920 system with microsecond μF900 xenon lamp excitation sources. Diffuse reflectance spectra (DRS) were recorded using a Cary 5000 UV-VIS-NIR spectrophotometer equipped with a double out-of-plane Littrow monochromator using $BaSO_4$ as a standard reference. Thermoluminescence(TL) glow curves were collected in a FJ-427A TL meter (Beijing Nuclear Instrument Factory) with the heating temperature range from 313 to 473 K. To release the energy stored in the material, the samples were pre-irradiated by using a 254 Xe lamp for 5 min and then heated at a linear rate of 2 K s^{-1}. Three-dimensional TL spectra were measured by using a RIS<DDA-15B/C TL/PL spectrometer. Immediately after being exposed for 5 min to an UV lamp with emission peaked at 254 nm (Gp3Hg-2, Fei Ying Light Electrical Appliance Factory), TL signals were recorded in the temperature range of 273-773 K and the heating rate was fixed at 5 K·s^{-1}. The EPR spectra were recorded on an EPR spectrometer (Bruker A300) operating in the X-band frequencies (−9.447 GHz) at 100 K, with the microwave power of 2.12 mW. CL spectra were detected using a modified RELIOTRON III CL instrument. Spectra data were recorded on an Ocean Optics USB4000 charge coupled device spectrometer. The CL photo was taken using iphone 6 plus. All the PL spectra were corrected for the wavelength-dependent response of the detector system, and for

comparison, the spectra were recorded under identical measurement conditions. Appropriate optical filters were employed to avoid any possible interference in all spectral measurements.

Experimental Procedures: A series of polycrystalline powder samples was prepared through a traditional solid state reaction.[18] The reactants include 99.99% $CaCO_3$, 99.999% Ga_2O_3, GeO_2, and 99.95% pure chromium sesquioxide Cr_2O_3. On the account of the nominal compositions of compounds $Ca_3Ga_{2-x}Cr_xGe_3O_{12}$ (x = 0, 0.005, 0.01, 0.03, 0.05, 0.07, 0.10), appropriate amount of starting materials was thoroughly mixed and ground, and subsequently the mixture was first heated to 900 °C for 2 h. After cooling down to room temperature, the as-obtained powder were reground and then calcined at 1200 °C for 6 h in air atmosphere to obtain the final products.

Acknowledgements

This work was supported by the Foundation of 2014 Hong Kong Scholars Program (XJ2014042, PolyU grant G-YZ55), the National Natural Science Foundation of China (Grant Nos. 21301043 and 11474241), the Research Grants Council of Hong Kong GRF (PolyU 153281/16P), Natural Science Foundation of Guangdong Province (2014A030313737), Distinguished Young Teacher Training Program in Higher Education of Guangdong, China (Yq2013114).

Received: ((will be filled in by the editorial staff))

Revised: ((will be filled in by the editorial staff))

Published online: ((will be filled in by the editorial staff))

References

[1] H. Mi, Y. Huang, Z. Lin, L. Zhang, G. Wang, *CrystEngComm* **2014**, 16, 763.

[2] P. Wagenblast, U. Morgner, F. Grawert, F. X. Kärtner, *Opt. Lett.* **2003**, 28, 1713.

[3] Y. Li, M. Gecevicius, J. Qiu, *Chem. Soc. Rev.* **2016**, 45, 2090.

[4] S. K. Singh, *RSC Adv.* **2014,** 4, 58674.

[5] B.-Y. Wu, H.-F. Wang, J.-T. Chen, X.-P. Yan, *J. Am. Chem. Soc.* **2011**, 133, 686.

[6] J. P. Hehir, M. O. Henry, J. P. Larkin, G. F. Imbusch, *J. Phys. C.: Solid State Phys.* **1974,** 7, 2241.

[7] F. Liu, Y. Liang, Z. Pan, *Phys. Rev. Lett.* **2014**, 113, 177401.

[8] F. Liu, W. Yan, Y.-J. Chuang, Z. Zhen, J. Xie, Z. Pan, *Sci. Rep.* **2013**, 3, 1554.

[9] Y. Katayama, B. Viana, D. Gourier, J. Xu, S. Tanabe, *Opt. Mater. Express* **2016**, 6, 1405.

[10] S. K. Sharma, A.Bessière, N.Basavaraju, K. R. Priolkar,L.Binet, B. Viana, D.Gourier, *J.Lumin.* **2014**, 155, 251.

[11] U. Caldiño G., M. Voda, F. Jaque, J. García Solé, A.A. Kaminskii, *Chem. Phys. Lett.* **1993**, 213, 84.

[12] U. R. Rodríguez-Mendoza, S. F. León-Luis, J. E. Muñoz-Santiuste, D. Jaque, V. Lavín, *J. Appl. Phys.* **2013**, 113, 213517.

[13] D. Jaque, U. Caldiño, J. J. Romero, J. García Solé, *J. Lumin.* **1999**, 83-84, 477.

[14] F. Ramos-Lara, D. Jaque, J. García-Solé, U. Caldiño G., *J. Phys.:Cond. Matter* **2000**, 12, L441.

[15] D. Jaque, J. García Solé, *Phys. Rev. B* **2004**, 70, 155116.

[16] D. Chen, Y. Chen, H. Lu, Z. Ji, *Inorg. Chem.* **2014**, 53, 8638.

[17] C. Liu, Z. Xia, M. S. Molokeev, Q. Liu, *J. Am. Ceram. Soc.* **2015**, 98, 1870.

[18] H. Lin, T. Yu, G. Bai, M-K. Tsang, Q. Zhang, J. Hao, *J. Mater. Chem. C* **2016**, 4, 3396.

[19] M. Chen, Z. Xia, M. S. Molokeev, T. Wang, Q. Liu, *Chem. Mater.* **2017**, 29(3), 1430.

[20] Z. Xia, S. Miao, M. Chen, M. Molokeev, Q. Liu, *Inorg. Chem.* **2015**, 54, 7684.

[21] M. A. F. M. da Silva, I. C. S. Carvalho, N. Cella, H. N. Bordallo, L. P. Sosman, *Opt. Mater.* **2013**, 35, 543.

[22] Y. Li, Y. Li, R. Chen, K. Sharafudeen, S. Zhou, M. Gecevicius, H. Wang, G. Dong, Y. Wu, X. Qin, J. Qiu, *NPG Asia Materials* **2015**, 7, e180.

[23] F. You, A. J. J. Bos, Q. Shi, S. Huang, P. Dorenbos, *Phys. Rev. B* **2012**, 85, 115101.

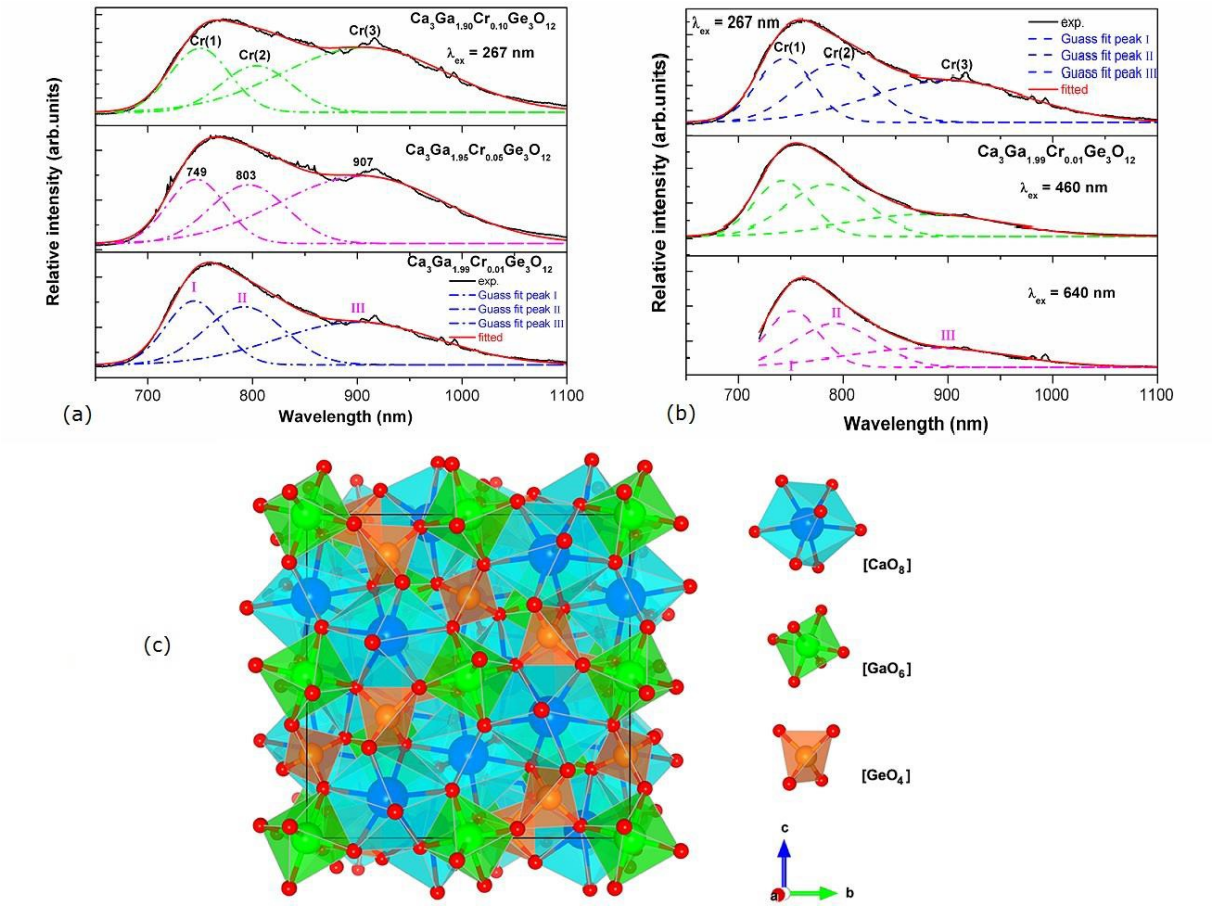

Figure 1. (a)The NIR emission spectra of the samples $Ca_3Ga_{2-x}Cr_xGe_3O_{12}$ (x = 0.01, 0.05, 0.10) under 267 nm excitation at RT. (b) The NIR emission spectra of the samples $Ca_3Ga_{1.99}Cr_{0.01}Ge_3O_{12}$ under 267, 460, 640 nm excitation at RT. (c) Schematic diagram of $Ca_3Ga_2Ge_3O_{12}$ structure and coordination environment of the Ca^{2+}, Ga^{3+}, and Ge^{4+} cations.

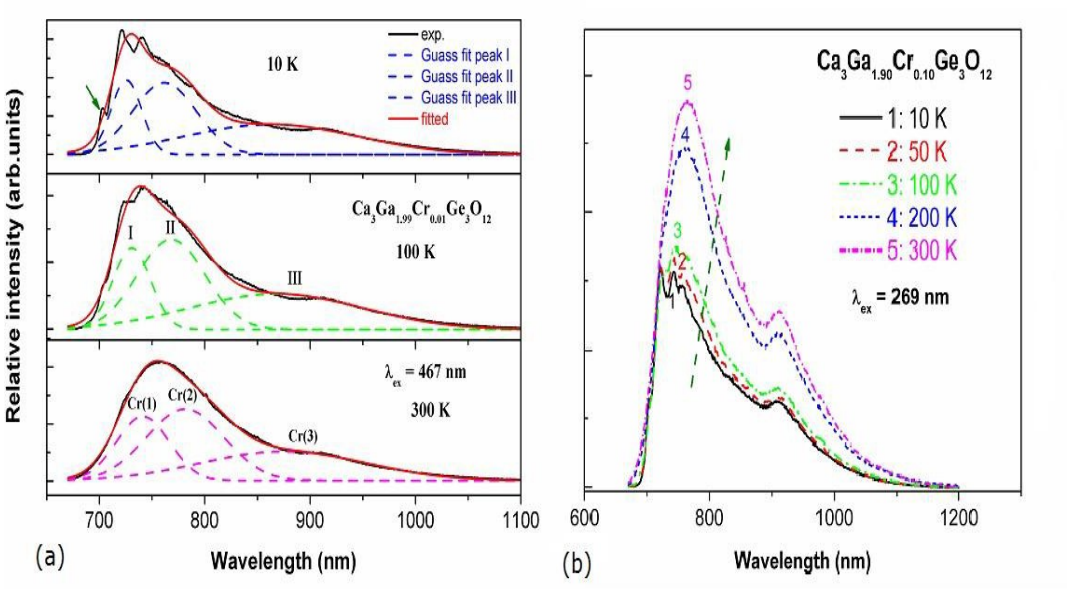

Figure 2. (a) The NIR emission spectra of the samples $Ca_3Ga_{1.99}Cr_{0.01}Ge_3O_{12}$ under 467 nm excitation at 10 K, 100 K, and 300 K, respectively. (b) Variable temperature emission spectra of $Ca_3Ga_{1.99}Cr_{0.01}Ge_3O_{12}$ using excitation at 269 nm.

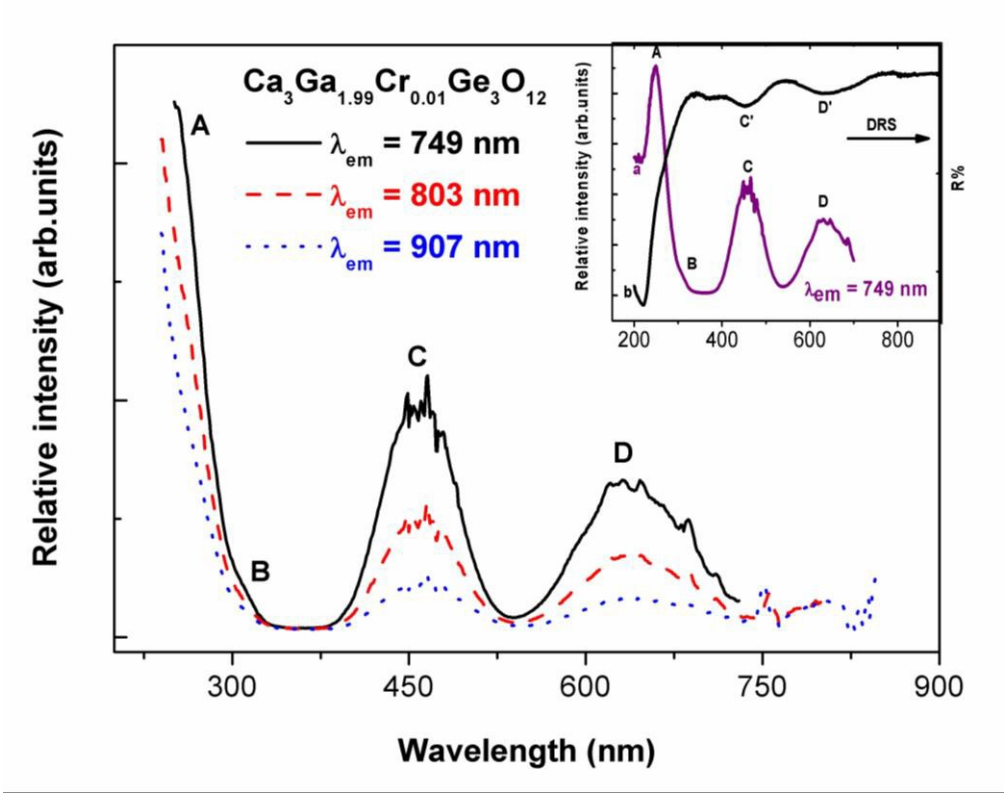

Figure 3. The excitation spectra of the sample $Ca_3Ga_{1.99}Cr_{0.01}Ge_3O_{12}$ under 749, 803, and 907 nm emissions at RT, respectively. The inset shows (a) the excitation spectrum of $Ca_3Ga_{1.99}Cr_{0.01}Ge_3O_{12}$ monitoring 749 nm emission at RT in the range of 200-700 nm, (b) the diffuse reflection spectrum of $Ca_3Ga_{1.99}Cr_{0.01}Ge_3O_{12}$.

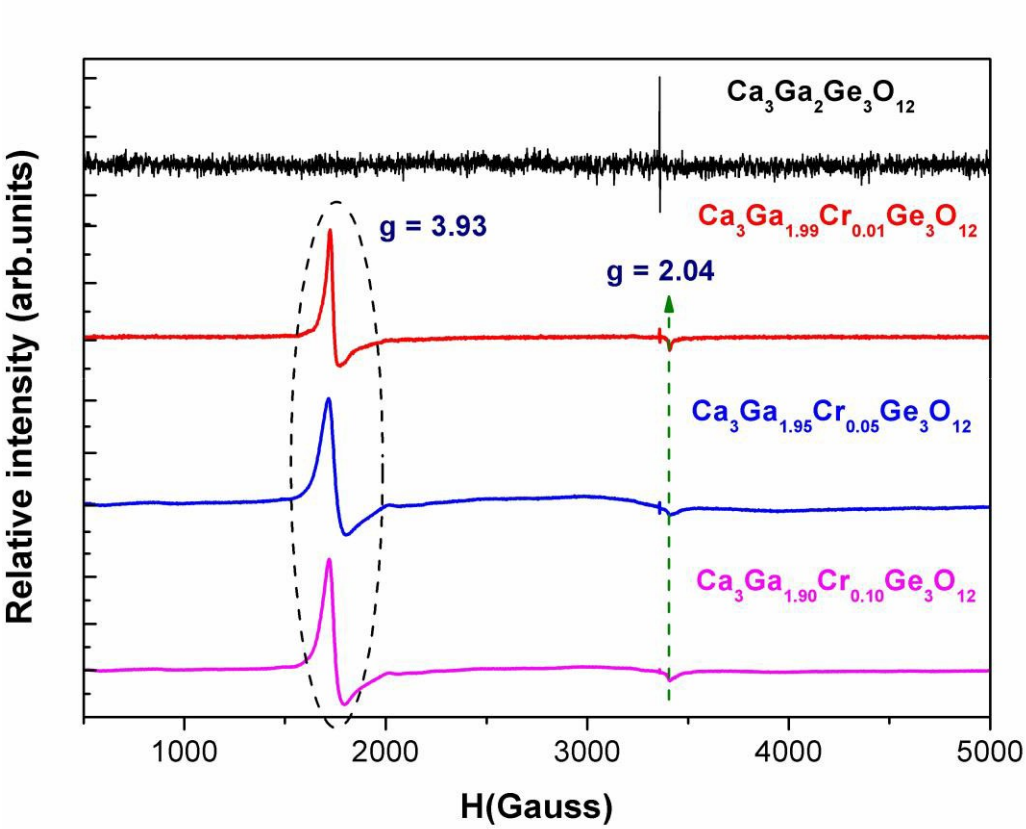

Figure 4. EPR spectra of the samples $Ca_3Ga_{2-x}Cr_xGe_3O_{12}$ (x = 0.01, 0.05, 0.10) measured at 100 K.

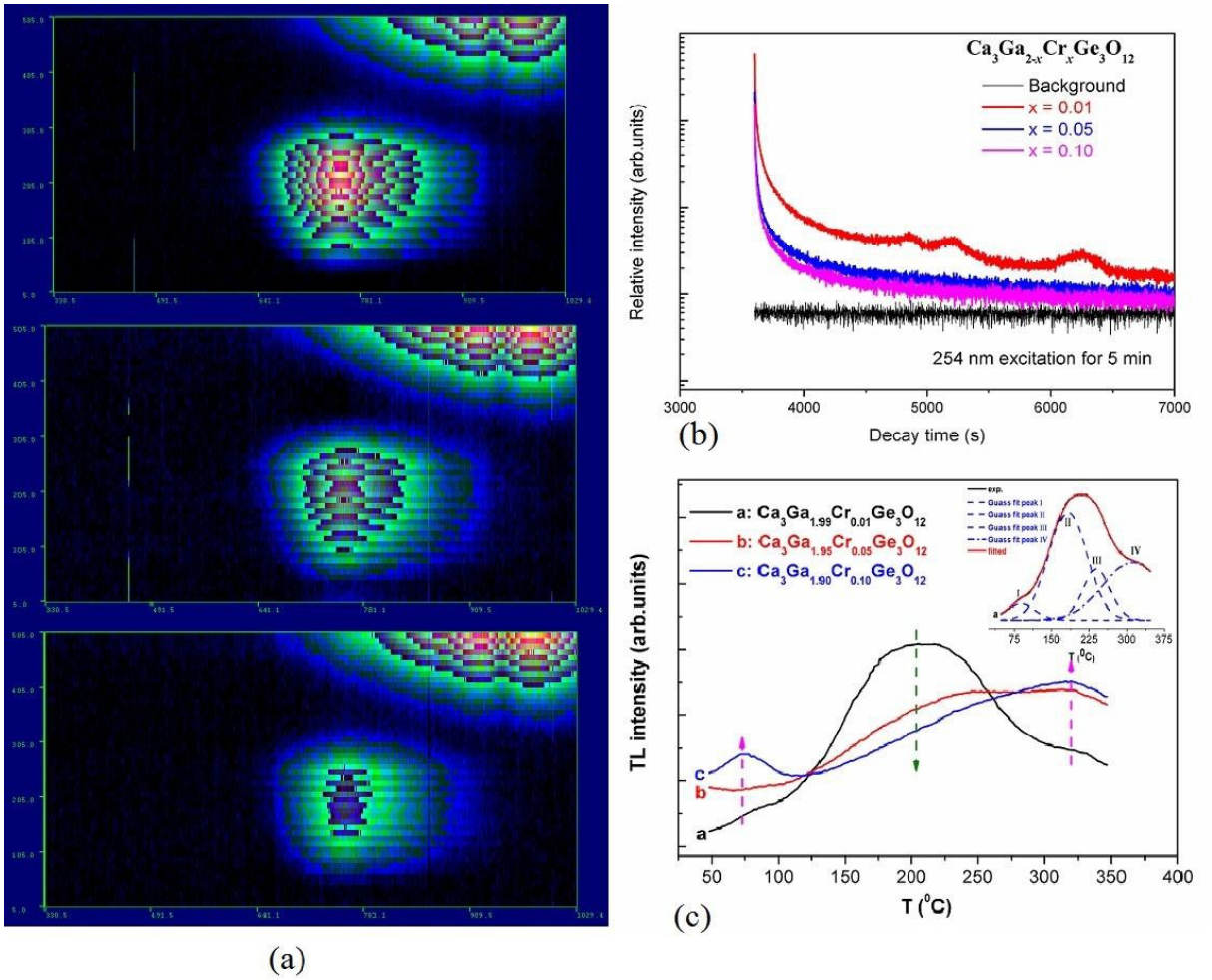

Figure 5. (a) Three-dimensional thermoluminescence spectra of the samples $Ca_3Ga_{2-x}Cr_xGe_3O_{12}$ (x = 0.01, 0.05, 0.10 from top to bottom) after 254 nm excitation for 5 min. (b) LLP decay curves of Cr: CGGG phosphors doped with various Cr^{3+} contents monitored at 750 nm emission after 254 nm light illumination for 5 min. (c) Thermoluminescence curves of the samples $Ca_3Ga_{2-x}Cr_xGe_3O_{12}$ (x = 0.01, 0.05, 0.10) after 254 nm excitation for 5 min. The inset shows the Gauss fit peaks of curve a corresponding the sample $Ca_3Ga_{1.99}Cr_{0.01}Ge_3O_{12}$.

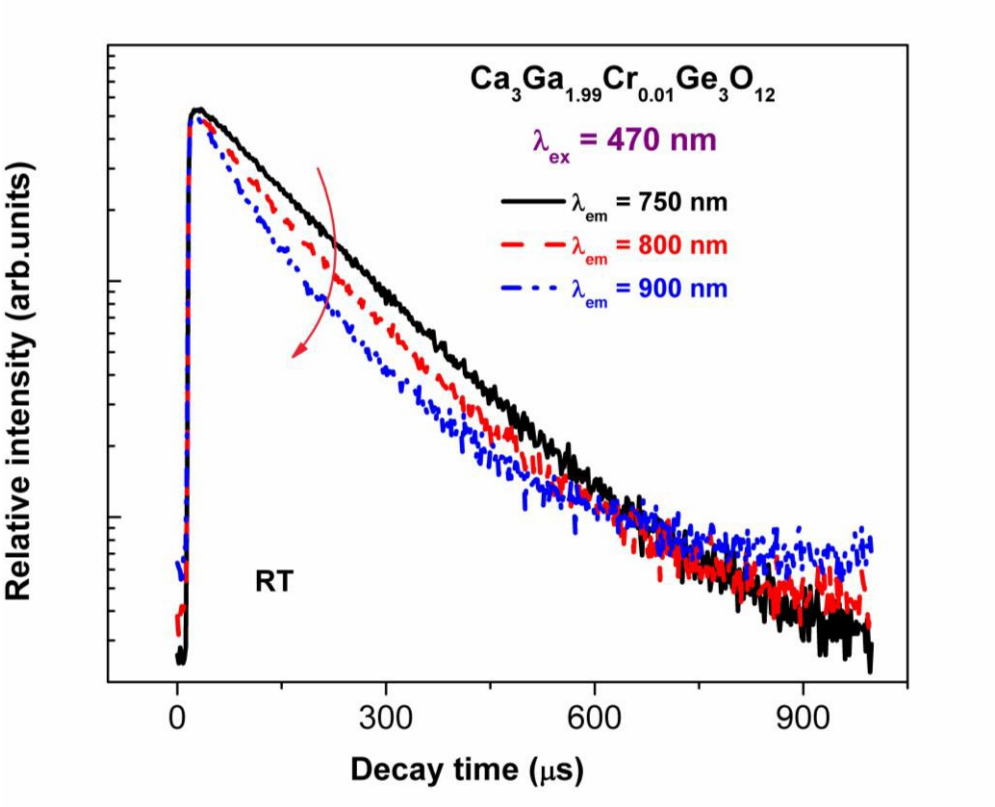

Figure 6. The decay curves of $Ca_3Ga_{1.99}Cr_{0.01}Ge_3O_{12}$ upon 470 nm excitation with different emission wavelength at RT.

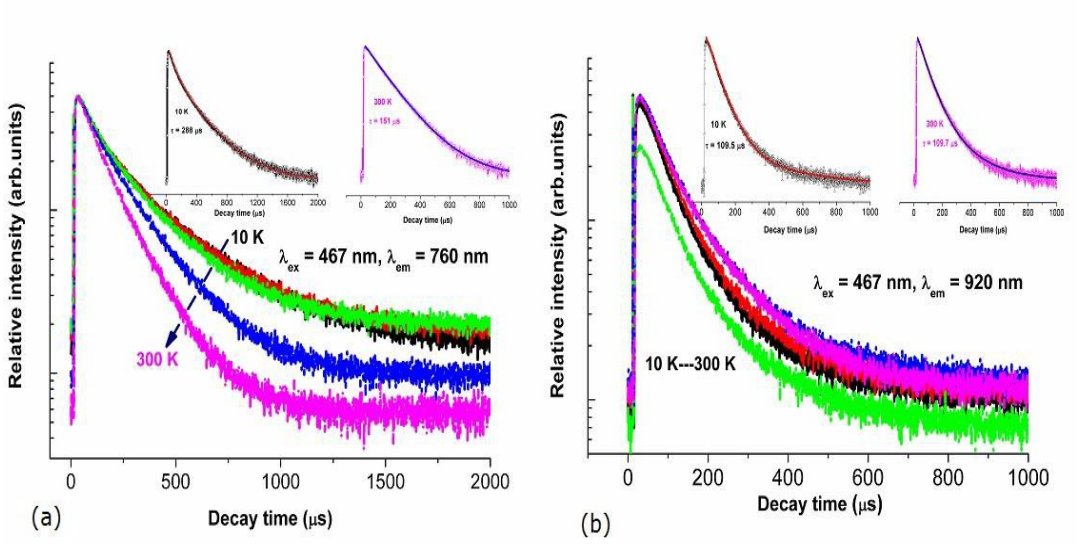

Figure 7. (a) The decay curves of $Ca_3Ga_{1.99}Cr_{0.01}Ge_3O_{12}$ upon 467 nm excitation with emission wavelengths at 765 nm in different temperature (10 K, 50 K, 100 K, 200 K, and 300 K). (b) The decay curves of $Ca_3Ga_{1.99}Cr_{0.01}Ge_3O_{12}$ upon 467 nm excitation with emission wavelengths at 900 nm in different temperature. The key is indicated in the inset of (a), (b).

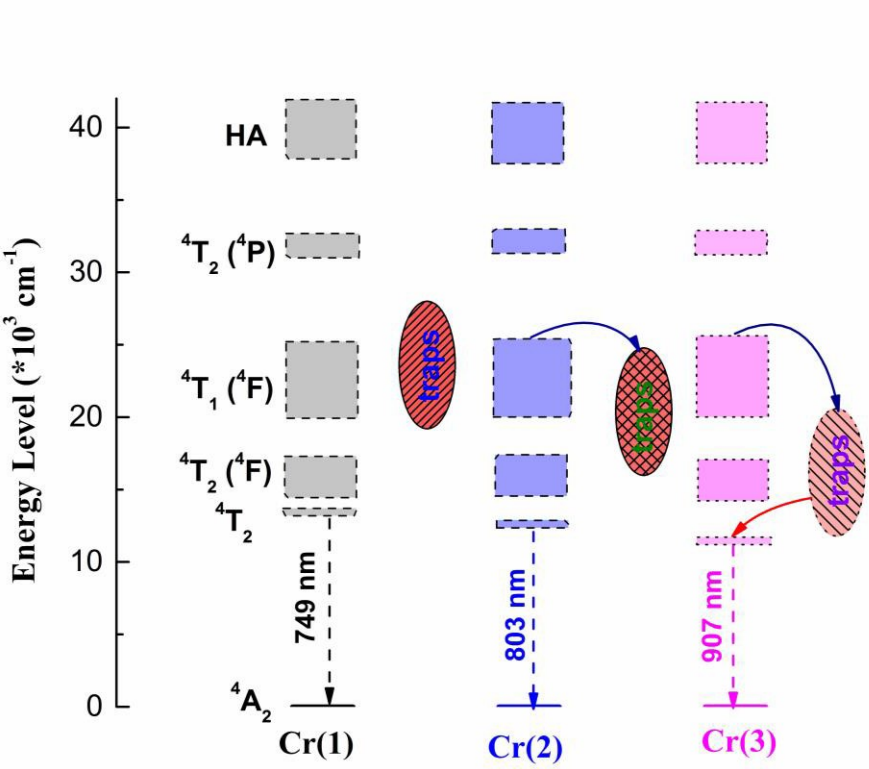

Figure 8. The schematic energy levels of Cr(1), Cr(2) and Cr(3) in $Ca_3Ga_2Ge_3O_{12}$: Cr^{3+}.

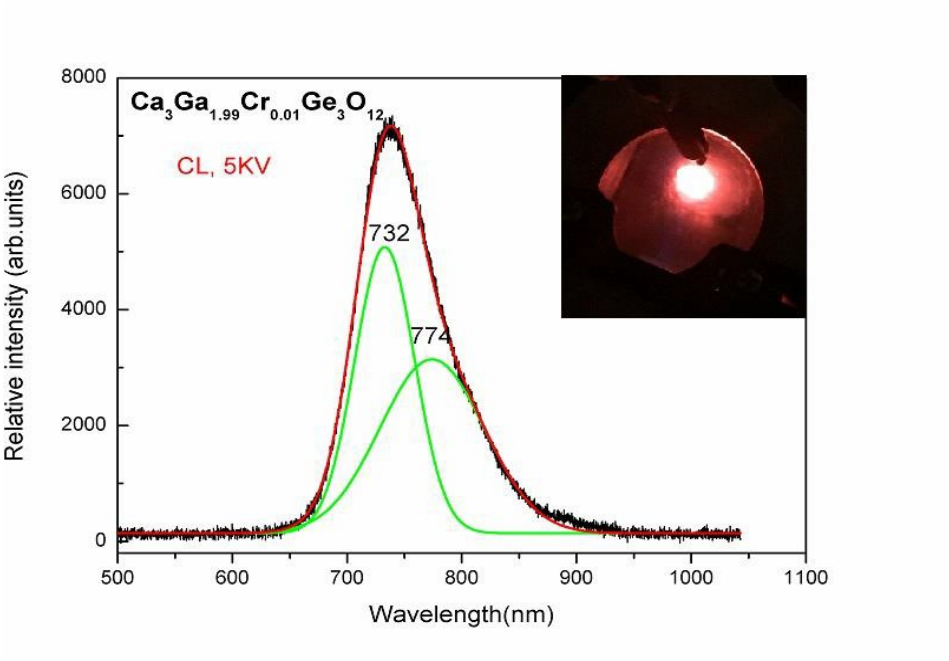

Figure 9. The emission spectrum of the sample $Ca_3Ga_{1.99}Cr_{0.01}Ge_3O_{12}$ under cathode-ray excitation. The inset shows the photo of $Ca_3Ga_{1.99}Cr_{0.01}Ge_3O_{12}$ under cathode-ray excitation with 5 KV power.

The table of contents

Persistent near-infrared luminescence properties of Cr^{3+} activated $Ca_3Ga_2Ge_3O_{12}$ have been studied under ultraviolet and visible light excitation. Through studying crystal field on site occupancy, energy transfer and the decay behaviors, it is found the traps formed by Cr^{3+} entering Ga^{3+} site produce superior persistent near-infrared luminescence. Three types of Cr^{3+} centers in $Ca_3Ga_2Ge_3O_{12}$ generate three near-infrared luminescence peaks.

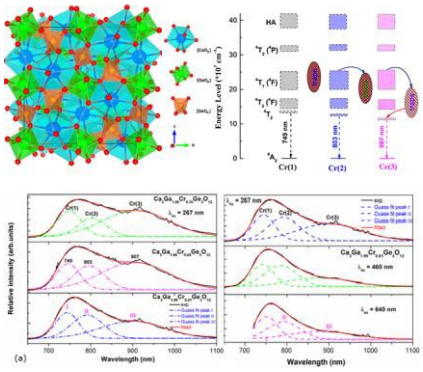

Dr. H.H. Lin, Dr. G.X. Bai, T. Yu, M.-K. Tsang, Prof. Q.Y. Zhang, Prof. J.H. Hao*

Site occupancy and near-infrared luminescence in $Ca_3Ga_2Ge_3O_{12}$: Cr^{3+} persistent phosphor